

# Forming Chemisorbed Single-Molecule Junctions through Loss of Stable Carbocations

Jazmine Prana, Luana Zagami, Kelly Yan, Daniel Hernangómez-Pérez,\* María Camarasa-Gómez,\* and Michael S. Inkpen\*



Cite This: <https://doi.org/10.1021/acs.nanolett.5c01893>



Read Online

ACCESS |

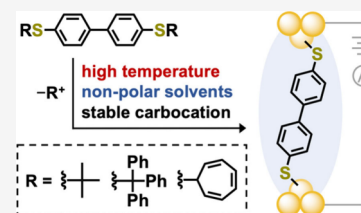
Metrics & More

Article Recommendations

Supporting Information

**ABSTRACT:** Recent studies have found that “chemically inert” gold surfaces may drive S–C( $sp^3$ ) bond cleavage reactions in thioether (–SR) linker groups, providing access to single-molecule junctions with chemisorbed Au–S contacts following the elimination of R<sup>+</sup>. Here, we demonstrate that such transformations occur more readily at elevated temperatures, rough surfaces, and in *nonpolar* solvents. We further show that a greater proportion of chemisorbed bonds are formed when R = –CPh<sub>3</sub> or –C<sub>7</sub>H<sub>7</sub> than when R = –<sup>t</sup>Bu, consistent with the relative stability of [<sup>t</sup>Bu]<sup>+</sup> < [CPh<sub>3</sub>]<sup>+</sup> ~ [C<sub>7</sub>H<sub>7</sub>]<sup>+</sup> carbocations. Our contact chemistry assignments are supported by first-principles transmission calculations, and we apply potential energy calculations to expose the relatively small influence of applied external electric fields on this bond breaking process. Together, this work provides a deeper understanding of reactivity at metal surfaces, of broad relevance to heterogeneous catalysis and critical to the stability and function of molecular junctions and monolayers.

**KEYWORDS:** *molecular electronics, single-molecule conductance, scanning tunneling microscope-based break junction method, DFT-NEGF, interfacial reactions, carbocation chemistry*



Interfacial bond-breaking and bond-forming processes form the basis of all heterogeneous catalytic processes used across chemical industry.<sup>1,2</sup> They also play an important role in anchoring molecular species to metal surfaces through chemisorption, enabling, for example, fundamental studies of electron transfer,<sup>3</sup> self-assembly,<sup>4</sup> or chemical reactivity,<sup>5</sup> as well as applications in biosensing<sup>6</sup> or catalysis.<sup>7</sup> A prototypical example in this context is the reaction of molecules comprising thiol (–SH) groups at the surface of gold to form adsorbed thiolates (–S–Au).<sup>8</sup> The resulting chemisorbed bonds are distinguished from structurally related physisorbed –S(R)–Au interactions, where the adsorbing thioether groups (–SR) do not undergo any significant chemical change. Such differences in surface bonding interactions can be readily evaluated using metal/single molecule/metal junctions, devices which approach the limit of miniaturization for circuit elements used in computation or data storage. Here, chemisorbed sulfur, carbon, nitrogen, and oxygen contacts to gold and/or silver electrodes, formed from reactive groups such as thiols,<sup>9,10</sup> trialkylstannanes,<sup>11</sup> alkynes,<sup>12,13</sup> amines,<sup>14</sup> carboxylic acids,<sup>15</sup> and halides,<sup>16,17</sup> have been widely exploited to form single-molecule junctions with distinct transport properties. These contact chemistries have also been used to study the influence of applied external electric fields, solvent environment, or electrochemical potential,<sup>16,18</sup> as well as temperature<sup>19</sup> on the competency and rate of chemical transformations occurring at electrode surfaces, using single-molecule conductance measurements to monitor reaction progress.

Recent reports have highlighted the possibility of forming junctions with chemisorbed Au–S bonds from components comprising thio-*tert*-butyl (–S<sup>t</sup>Bu)<sup>20,21</sup> or 2,3-dihydrobenzo-[b]thiophene<sup>22</sup> linker groups. For 4,4′-bis(*tert*-butylthio)-1,1′-biphenyl (<sup>t</sup>Bu, Figure 1), it was proposed that coordination of the sulfur lone pair of –S<sup>t</sup>Bu (a Lewis base) to an undercoordinated, electropositive, gold atom (serving as a Lewis acid) activates the S–C( $sp^3$ ) bond toward heterolytic cleavage.<sup>20,23</sup> In this scheme, –S–Au is formed from –S(<sup>t</sup>Bu)–Au with the concurrent loss of [<sup>t</sup>Bu]<sup>+</sup>, a moderately stable tertiary carbocation.<sup>24</sup> This draws analogies to established solution-based reactions in which –<sup>t</sup>Bu groups can be cleaved from –S<sup>t</sup>Bu in the presence of Lewis acids such as TiCl<sub>4</sub>/BBr<sub>3</sub>.<sup>25,26</sup> Importantly, analogous S–C( $sp^3$ ) bond breaking processes were not observed in studies of related components comprising –SR linkers with substituents that would form less stable primary/secondary carbocations through such reactions.<sup>20</sup> These studies raise several additional questions, most notably: (1) what are the key factors influencing such surface-mediated bond breaking processes; (2) can additional evidence be presented in support of the proposed (carbocation loss) mechanism; and (3) does this

**Received:** March 26, 2025

**Revised:** June 5, 2025

**Accepted:** June 9, 2025

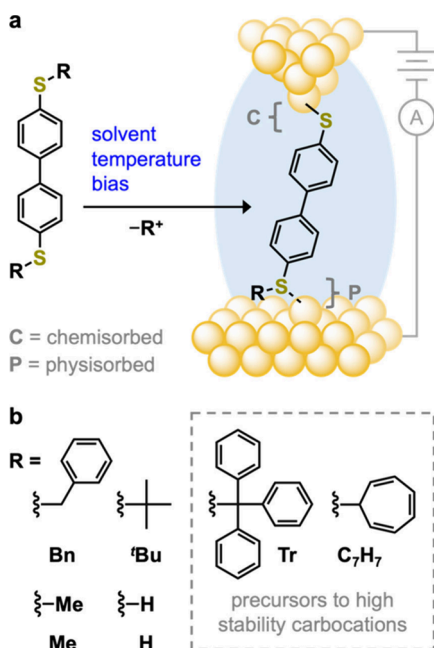


**Figure 1.** *In situ*  $S-C(sp^3)$  bond breaking reactions at the surface of gold electrodes are studied using molecular conductance measurements. (a) Single-molecule junctions (right) are formed from solution using molecular analytes comprising a 4,4'-biphenyl backbone functionalized with different thioether/thiol linkers ( $-SR$ ; left). While thioether linkers are typically used to form physisorbed (P) contacts to gold electrodes, they may also yield chemisorbed (C) contacts when  $R^+$  is an appropriate leaving group. (b) Molecular structures of the R groups for each compound studied here. These thioethers would be expected to generate carbocations of different stabilities following heterolytic  $S-C(sp^3)$  bond cleavage. Complete molecular structures of all analytes and solvents are provided in Figure S1. Using  $tBu$  (where  $R = -tBu$ ), we probe the influence of solvent, temperature, and junction voltage bias ( $V_{bias}$ ) on this interfacial bond-breaking process.

reactivity impact the interpretation of any previous investigations in molecular electronics involving thioether-substituted compounds? For completeness, we note that these reactions bear similarities to *in situ*  $Si-C(sp)$  bond cleavage processes observed with trimethylsilyl alkyne-based linker groups ( $Me_3Si-C\equiv C-$ ).<sup>12,27</sup>

Accordingly, here we present an expansive study that evaluates the impact of different reaction conditions and thioether substituents on the formation of chemisorbed contacts in model single-molecule junctions. Using  $tBu$ , we find that *in situ*  $S-C(sp^3)$  cleavage is favored at elevated temperatures, rough surfaces, and, perhaps surprising, in *nonpolar* solvents. In contrast, the junction voltage bias ( $V_{bias}$ ) appears to play a relatively minor role; potential energy calculations of  $S-C(sp^3)$  bond breaking reveal that applied external electric fields only weakly perturb the barrier height. We next study analogous junction components comprising  $-SR$  linkers designed to form carbocations of much greater stability than  $[tBu]^+$  after heterolytic  $S-C(sp^3)$  bond cleavage:  $R =$  triphenylmethyl (Tr; forming the tritylium cation,  $[CPh_3]^+$ ) or cycloheptatrienyl ( $C_7H_7$ ; forming the tropylium cation,  $[C_7H_7]^+$ ). Molecular structures of all analytes and solvents are provided in Figure 1b and Figure S1. In strong support of the hypothesized reaction mechanism, and in contrast to measurements using  $tBu$ , both compounds *exclusively* form chemisorbed junctions. Finally, we show that

a component with  $R =$  benzyl (Bn) forms only physisorbed junctions, indicating that benzyl cations ( $[PhCH_2]^+$ ) are not eliminated under common measurement conditions. First-principles transmission calculations confirm that physisorbed (intact)  $tBu$ , Tr,  $C_7H_7$ , and Bn junctions should exhibit a lower conductance than for analogous junctions with chemisorbed contacts; supporting the assignment of high conductance  $tBu$ , Tr, and  $C_7H_7$  features found experimentally to junctions with chemisorbed contacts.

We perform conductance measurements using the scanning tunneling microscope-based break junction (STM-BJ) method<sup>9,28</sup> with custom-built instrumentation described previously (see the SI).<sup>19,29,30</sup> Briefly, we apply a  $V_{bias}$  between a gold STM tip and substrate and measure the current ( $I$ ) as the tip is pushed in and out of electrical contact. We plot the conductance ( $G = I/V_{bias}$ ) as a function of tip-substrate displacement, obtaining traces that comprise step features around integer multiples of the conductance quantum ( $G_0 = 7.748 \times 10^{-3}$  S). These features are attributed to the formation and breaking of atomic-sized gold contacts. After introducing 4,4'-biphenyl-based analytes as 0.1–1 mM solutions in various solvents, we observe new step features in these traces below 1  $G_0$  that correspond to the formation of single-molecule junctions (Figure 1a). We compile thousands of consecutively measured traces into one-dimensional (1D) conductance and two-dimensional (2D) conductance-displacement histograms (constructed without data selection), whereby the individual steps combine to form conductance features that are further analyzed to determine the most probable characteristics of the molecular junction. Synthetic methods for all noncommercially available 4,4'-biphenyl compounds are described in the SI.

We first present, in Figure 2b–e, overlaid 1D histograms for measurements of  $tBu$  in different solution environments. Each histogram exhibits between 1 and 3 prominent conductance features, which we assign to junctions comprising two physisorbed contacts (PP, low conductance), one physisorbed and one chemisorbed contact (PC, medium conductance), or two chemisorbed contacts (CC, high conductance; Figure 2a). These peak assignments follow those made for previous studies of  $tBu$  in 1,2,4-trichlorobenzene (TCB), after accounting for small changes in conductance attributed to solvent effects.<sup>31</sup> While we observe experiment-to-experiment variation in the relative intensities of each peak (Figures S6, S7), the data presented here exposes key trends in interfacial reactivity after appropriate analysis (Figure S2). Specifically, we deconvolute each histogram into three Gaussian peaks (Figure S3) then use the peak areas to calculate the percentage of chemisorbed contacts (%C; Tables S1, S2). This quantitative metric facilitates straightforward comparisons of different measurements. We attribute the experimental variation in measurements of  $tBu$ , in part, to differences in surface roughness near the junction that influence the local concentration of chemisorbed species generated at undercoordinated Lewis acidic atoms.<sup>26</sup> Where lateral tip-substrate drift is low, repeated tip-substrate contact will significantly increase the surface roughness around the junction.<sup>32</sup> While it is not trivial to routinely standardize these experimental parameters, this hypothesis is supported here through measurements utilizing substrates of different surface roughness and methods to maximize/minimize tip-substrate drift (Figure S4).

We contrast representative data from measurements in the nonpolar solvents tetradecane (TD), mesitylene (mes), and squalane (SQ; Figure 2b, c), against those in polar solvents 1-

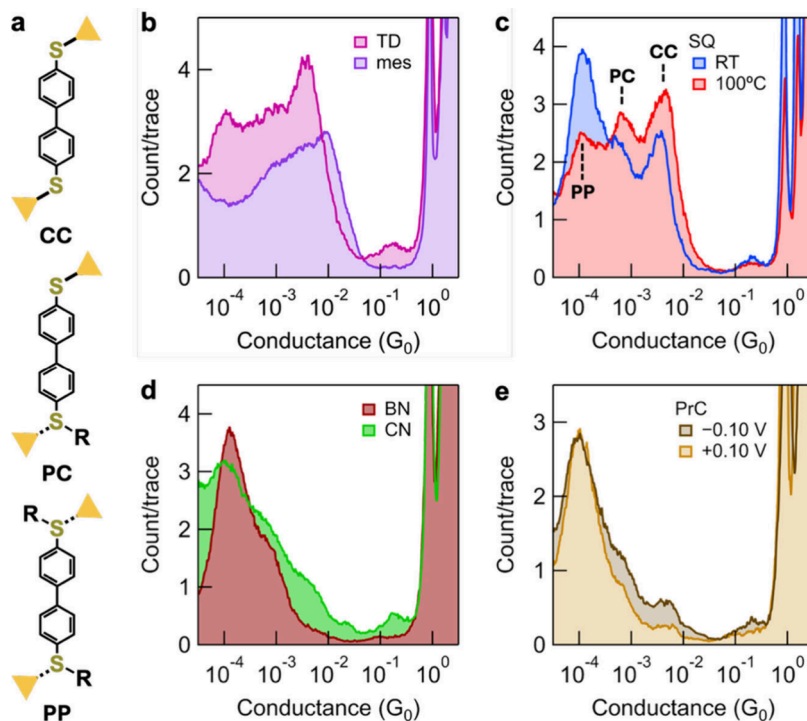


**Figure 2.** (a) Schematic illustration of CC, PC, and PP junction geometries (for  ${}^t\text{Bu}$ ,  $\text{R} = -{}^t\text{Bu}$ ). (b–e) Overlaid 1D conductance histograms obtained for measurements of  ${}^t\text{Bu}$  performed under different conditions (5000 traces,  $V_{\text{bias}} = 0.10$  V unless stated). Data from repeated measurements are provided in Figures S6 and S7, with a summary of analyzed data sets provided in Figure S2. Representative 2D conductance-displacement histograms are shown in Figure S5. Measurements in nonpolar solvents such as tetradecane (TD), squalane (SQ; dipole moment,  $\delta \sim 0$  D, dielectric constant,  $\epsilon \sim 2^{33}$ ), or mesitylene (mes;  $\delta = 0$  D,  $\epsilon = 2.28^{34}$ ) are provided in panels (b) and (c). These exhibit a relative high proportion of conductance peaks associated with PC and CC junction geometries (a high percentage of chemisorbed contacts, %C), although the relative intensity of each peak varies with experiment. Measurements in SQ consistently exhibit a larger %C after heating solutions to 100 °C. In contrast, measurements in polar solvents such as 1-bromonaphthalene (BN;  $\delta = 1.55$  D,  $\epsilon = 4.77$ ), 1-chloronaphthalene (CN;  $\delta = 1.57$  D,  $\epsilon = 5.04$ ), or propylene carbonate (PrC;  $\delta = 4.9$  D,  $\epsilon = 66.14$ ), shown in panels (d) and (e), yield histograms that predominantly comprise PP features (low %C).<sup>34</sup>

bromonaphthalene (BN), 1-chloronaphthalene (CN), and propylene carbonate (PrC; Figure 2d, e). This comparison, supported by an analysis of repeated, completely independent, measurements summarized in Figure S2a, shows we consistently obtain %C > 38% in nonpolar solvents and %C < 38% in polar solvents. The apparent decreased interfacial reactivity of  ${}^t\text{Bu}$  in solvents of higher polarity is perhaps surprising, given the well-established trends for reactions involving carbocation intermediates in bulk solution.<sup>35</sup> In the bulk, polar solvents help to stabilize charged intermediates, decreasing the activation barrier and so increasing the reaction rate. We also consistently observe an increase in %C for measurements in SQ after heating the same solution and substrate used at room temperature to 100 °C (Figure 2c, Figure S2b). We attribute this result to the more frequent higher energy molecular collisions that occur at elevated temperatures which can overcome the activation barrier for the interfacial reaction.

In rationalizing these observations, we note some key features of these surface-mediated solution-based reactions that distinguish them from bulk solution processes. *First*, where bond-breaking/forming steps occur at specific surface sites, the activity and accessibility of these sites may be moderated by other components of the system. For example, any dissolved water may serve as a competing Lewis base for the Lewis acidic undercoordinated gold adatoms,<sup>30,36,37</sup> or activated surface-adsorbed water ( $[(\text{HO}^{\delta-}-\text{Au}^{\delta+})\text{H}^{\delta+}]$  sites,<sup>38</sup> thought to

mediate  $\text{S}-\text{C}(sp^3)$  bond breaking. Hydrophobic solvents such as TD, mes, and SQ will poorly solubilize adventitious water, and evaporative loss of adventitious water is expected at elevated temperatures, contributing to an increased %C. Furthermore, TD, mes, and SQ do not themselves comprise any coordinating atoms that can interact with these sites (in contrast to the O, Cl, Br atoms of PrC, CN, and BN).<sup>31</sup> The modulation of reaction rates, and even selectivity, through solvent interactions or adsorbates on heterogeneous catalyst surfaces, is well-documented.<sup>39,40</sup> *Second*, a conducting metal substrate can itself serve to effectively solvate and stabilize proximal charged species (or dipoles) through polarization of the delocalized electrons in the bulk.<sup>41,42</sup> Stated differently, a metal surface may serve to lower activation barriers associated with the formation of charged intermediates even when reactions are performed in air, vacuum, or a low dielectric solvent.

We next evaluate the influence of the applied external electric field on the *in situ*  $\text{S}-\text{C}(sp^3)$  bond breaking process. Here we initially focused on measurements in TD as these support a moderate baseline reactivity and because the low dielectric of this medium will minimize screening of the field.<sup>43,44</sup> In Figure 3a, we plot histograms obtained from sequential solution measurements of  ${}^t\text{Bu}$  at  $V_{\text{bias}} = 0.10, 0.75,$  and  $0.10$  V in air. As evidenced from this data, and repeated measurements presented in Figure S6 (summarized in Figure S2b), we cannot clearly discern the influence of field strength

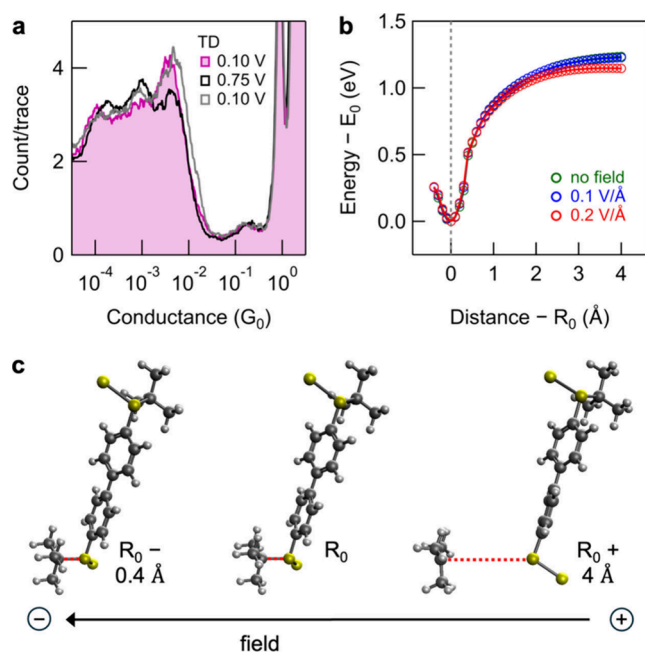


**Figure 3.** (a) Overlaid 1D histograms obtained from studies of **tBu** in TD measured sequentially at  $V_{\text{bias}} = 0.10, 0.75,$  and  $0.10$  V (each 5000 traces). 2D histograms corresponding to these measurements are provided in Figure S8. For repeated measurements and further analysis, see Figures S6a–e and S2b. We find that the field does not exert a discernible influence on the proposed interfacial S–C( $sp^3$ ) bond breaking reaction that leads to the formation of PC and CC junction geometries, at least within the experimental error of our measurements. (b) Overlaid plots of distance against the calculated total energy for **tBu**–Au<sub>1</sub> (see panel (c) for geometries), normalized to the equilibrium bond length ( $R_0$ , dashed line) and the equilibrium energy ( $E_0$ ), respectively. For each plot, a different electric field is applied along the S–C( $sp^3$ ) bond, as indicated by the arrow in panel (c). For this reaction model, the field appears to exert only a small influence on the height of the energy barrier to bond dissociation. (c) Optimized molecular geometries for **tBu**–Au<sub>1</sub> (applied field = 0 V/Å), obtained after constraining the distance between one S–C( $sp^3$ ) bond (dotted red lines) to different values relative to  $R_0$ . The *tert*-butyl group is observed to planarize upon dissociation, as expected for the carbocation.<sup>45</sup>

on %C under these conditions. Preliminary attempts to perform measurements of **tBu** in anhydrous TD solutions under an inert  $N_2$  atmosphere (inside of a glovebox) have also not yet provided any conclusive evidence that a larger applied field increases the apparent rate of this interfacial bond breaking reaction.

To clarify the effect of the field on this interfacial reaction, we turn to density functional theory (DFT) calculations using **tBu**–Au<sub>1</sub> a model comprising **tBu** with a single gold atom connected to each sulfur group (Figure 3b, c). Following a recently reported method,<sup>46</sup> we calculate the total energy of **tBu**–Au<sub>1</sub> after geometry optimization while constraining the distance between the S–C( $sp^3$ ) atoms in one –S<sup>t</sup>Bu group (see the SI for additional details). By compressing and stretching this bond, we obtain a bond dissociation curve (green line, Figure 3b) that resembles a Lennard-Jones potential. We subsequently repeat these calculations with a field of 0.1 V/Å and 0.2 V/Å along the constrained S–C axis. In agreement with our experimental observations, we find the field exerts only a small influence on the height of the energy barrier to bond dissociation, which decreases by  $\sim 7$  meV from

0 to 0.1 V/Å, and by 82 meV from 0.1 to 0.2 V/Å. While the barrier calculated here is large, we reason that this will be smaller in experiments due to the presence of solvent and the proximal polarizable electrode. Furthermore, the conductance signal of products formed is likely amplified by their chemisorption on the surface even for slow reactions (they cannot easily diffuse away into the bulk).<sup>22</sup> For completeness, we note that our bond dissociation curves do not comprise the transition state features that may be expected for such  $S_N1$ -like reaction coordinates. The observation of these features in related calculations, for example, that follow the formation of **tBuOH** from **tBuCl**, requires the inclusion of explicit solvent molecules.<sup>47</sup>

We subsequently targeted additional experiments using **Tr** and **C<sub>7</sub>H<sub>7</sub>** junction components (Figure 1b) to corroborate the proposed carbocation-loss mechanism for forming chemisorbed –S–Au contacts from **tBu**. These components comprise thioether groups capable of forming [CPh<sub>3</sub>]<sup>+</sup> and (aromatic) [C<sub>7</sub>H<sub>7</sub>]<sup>+</sup>, among the most stable carbocations known due to their extended,  $\pi$ -conjugated structures which stabilize the positive charge through resonance (*more stable* than [tBu]<sup>+</sup>).<sup>24,48</sup> We reasoned that if the rate of S–C( $sp^3$ ) bond cleavage is strongly influenced by carbocation stability, **Tr** and **C<sub>7</sub>H<sub>7</sub>** should form junctions with a greater proportion of chemisorbed contacts than **tBu**. In Figure 4a, we plot overlaid 1D histograms from measurements of **Tr** and **C<sub>7</sub>H<sub>7</sub>** in TCB. Each exhibits a single conductance peak at  $\sim 5 \times 10^{-3} G_0$  and  $\sim 1 \times 10^{-2} G_0$ , respectively. These values are greater than or equal to the conductance of junctions formed from biphenyl-4,4'-dithiol (**H**; R = H;  $\sim 5 \times 10^{-3} G_0$ ), a species recognized to form chemisorbed junctions in solution,<sup>10</sup> and higher than the most conducting 4,4'-biphenyl junctions with physisorbed –S(R)–Au contacts ( $\leq 2.5 \times 10^{-3} G_0$ ).<sup>20</sup> This result indicates that both **Tr** and **C<sub>7</sub>H<sub>7</sub>** exclusively form junctions with chemisorbed contacts, in strong support of the proposed *in situ* reaction mechanism (Figure S10). We emphasize here for clarity that no deprotection agents are added in these measurements, which are performed using standard STM-BJ methods. Interestingly, junctions formed from **C<sub>7</sub>H<sub>7</sub>** reproducibly exhibit a more intense peak feature with a conductance  $\sim 2\times$  higher than those formed from **H** (Table S3, Figure S13b); an unexpected result that warrants additional study (Figure S12a).

Finally, we explored the potential for **Bn** to undergo similar S–C( $sp^3$ ) bond breaking reactions at a gold surface. While the direct formation of primary benzyl cations ([PhCH<sub>2</sub>]<sup>+</sup>) might appear energetically unfavorable, these are reported to exhibit a similar thermodynamic stability to [tBu]<sup>+</sup> in the gas phase,<sup>24</sup> and the possibility that these species may undergo rearrangements to the ultrastable [C<sub>7</sub>H<sub>7</sub>]<sup>+</sup> has long been debated.<sup>49,50</sup> Crucially, **Bn** comprises the same aryl–CH<sub>2</sub>SR' (R' = H, Me) motif used elsewhere in molecular electronics, with assumed stability, to electronically decouple electrode and molecular backbone states,<sup>51–54</sup> or probe constructive quantum interference (Figure S11).<sup>55</sup> As shown in Figures 4a and S12b,c, measurements of **Bn** exhibit a single peak at a conductance significantly lower than the chemisorbed and physisorbed junctions formed from **H** and 4,4'-bis(methylthio)-1,1'-biphenyl (**Me**; R = Me), respectively. Following previous reports, we attribute the lower conductance of **Bn** junctions to the relatively bulky benzyl substituent, which enforces junction geometries that electronically decouple the electrode and molecular backbone states (discussed further below).<sup>20,56,57</sup>

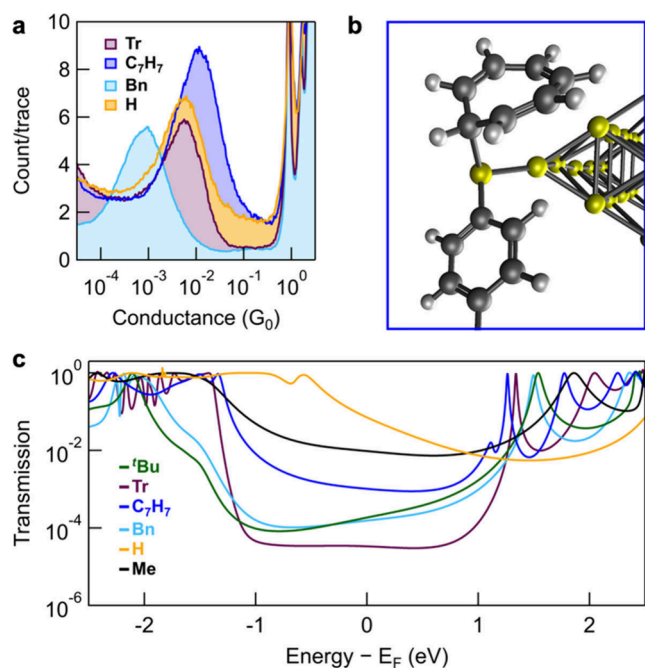


**Figure 4.** (a) Overlaid 1D histograms obtained from measurements of Tr,  $C_7H_7$ , Bn, and H as pure 0.1–1 mM solutions in 1,2,4-trichlorobenzene (TCB; 10,000 traces,  $V_{\text{bias}} = 0.1$  V). Histograms for Tr and  $C_7H_7$  exhibit single conductance peaks at or just above the conductance of H, a compound that is recognized to form Au–S chemisorbed contacts. In contrast, histograms for Bn show a single feature at  $>5\times$  lower conductance than H junctions. The 2D histograms corresponding to these measurements are provided in Figures S9. Data for H is reproduced from ref 20. (b) Optimized geometry for  $C_7H_7$  junctions, showing a close-up view of the physisorbed contact. Additional geometries for all modeled junctions are shown in Figure S15. (c) Overlaid DFT-NEGF transmission calculations. In contrast to our experimental findings for Tr and  $C_7H_7$ , all intact thioethers with physisorbed  $-S(R)-Au$  contacts exhibit a lower calculated conductance relative to H modeled with chemisorbed  $-S-Au$  bonds. Together, this data supports the hypothesis that Tr and  $C_7H_7$  exclusively form junctions with CC geometries (following  $S-C(sp^3)$  cleavage and loss of tritylium/tropylium cations), whereas Bn exclusively forms junctions with PP geometries (no  $S-C(sp^3)$  cleavage occurs (Figure S11)). We note that the low calculated conductance for physisorbed 'Bu junctions is in good agreement with the low experimental conductance peak features assigned to PP geometries (e.g., Figure 2d, e), and the results of earlier work.<sup>20</sup>

This implies that Bn forms only physisorbed junctions, and that this  $S-C(sp^3)$  bond is stable during conductance measurements. Our assignments of a PP geometry for Bn, and CC geometries for Tr and  $C_7H_7$ , are also supported by conductance noise analyses (Figure S14). In line with previous observations,<sup>10,22</sup> the average conductance noise is consistently larger for Bn and Me (physisorbed) junctions than for Tr,  $C_7H_7$ , and H (chemisorbed) junctions.

To further evaluate our experimental observations we turn to *ab initio* quantum transport calculations conducted within the framework of DFT and the nonequilibrium Green's function (NEGF) formalism, utilizing FHI-aims<sup>58</sup> in conjunction with the AITRANSS transport module (see the SI for additional details).<sup>59–61</sup> In Figure 4c, we display overlaid transmission calculations for 'Bu, Tr,  $C_7H_7$ , Bn, H, and Me model junctions. A representative optimized geometry for  $C_7H_7$  is shown in Figure 4b, giving a clear view of the

physisorbed contact, with additional junction geometries provided in Figure S15. We focus here on the trends in calculated conductance rather than their absolute values, which are overestimated by  $>1$  order of magnitude due to the well-known inherent limitations of generalized-gradient approximations applied in this context.<sup>62,63</sup>

We first observe that H, despite having the largest gas phase HOMO–LUMO gap (Table S5), exhibits the highest conductance. Here, transport is strongly dominated by the HOMO, which is broadened due to chemisorption and increased coupling with the electrode (CC geometry). Notably, all other physisorbed junctions (PP geometries) exhibit a lower conductance, with the Fermi level ( $E_F$ ) positioned approximately at the midpoint of each HOMO–LUMO gap. The trends in calculated conductance for H (CC)  $>$  Me (PP)  $>$  Bn (PP)  $\sim$  'Bu (PP) agree well with those assigned experimentally (Figures 2, 4a, and Figure S12b). The calculated conductance of PP junctions also inversely correlates with the steric bulk of R (i.e.,  $Me \gg$  'Bu, Bn,  $C_7H_7$ , Tr), as noted previously.<sup>20,57</sup> A closer inspection of each junction geometry (Figure S15, Table S4) reveals the Au–S bond of physisorbed contacts for all junctions except the sterically unhindered H and Me is misaligned with, and so electronically decoupled from, the conjugated backbone  $\pi$ -orbitals. This decoupling can be seen in the transmission calculations, where the unoccupied resonances of Me are broadened relative to those for all other physisorbed junctions, which decreases their transmission at  $E_F$ .

The low calculated conductance for Tr and  $C_7H_7$  (PP geometries) contrasts sharply with our experimental findings that the conductance of junctions formed from these compounds and H differ only by a factor of  $\sim 2$ . Importantly, this discrepancy supports our assertion that, under experimental conditions, the  $S-C(sp^3)$  bonds in Tr and  $C_7H_7$  break to form chemisorbed Au–S contacts. Similarly, the low calculated conductance of 'Bu (PP) supports assignment of the higher conductance peaks in measurements of 'Bu to junctions of the PC/CC type. In closing, we note that our model Tr junctions necessarily involve a frozen geometry (Figure S15). When performing calculations using strict energy and force convergence criteria, all relaxed geometries for Tr show that the  $S-C(sp^3)$  bond spontaneously cleaves after attaching the gold clusters. This observation further highlights the propensity of this  $S-C(sp^3)$  bond to break in STM-BJ experiments.

In conclusion, we have shown that the most effective conditions to drive thioether  $S-C(sp^3)$  bond cleavage using gold electrodes involve nonpolar solvents, atomically rough surfaces, and elevated temperatures, while the applied electric field appears to play a relatively minor role. It is anticipated that these conditions will prove useful in future studies where the identification of, or control over, such Lewis acid-mediated reactions in single-molecule junctions, self-assembled monolayers,<sup>64</sup> or heterogeneous catalytic processes is important. Critically, the exclusive formation of chemisorbed junctions in measurements of Tr and  $C_7H_7$ , in contrast to the distinct junction geometries formed from 'Bu, strongly implicate that the stability of the carbocation leaving group increases the apparent rate of this interfacial reaction. This provides additional support for the carbocation intermediates proposed in reaction mechanisms involving these (Figure S10) and other compounds.<sup>20</sup> Given that many other chemical groups may function as stable carbocations,<sup>48</sup> our observations present new

opportunities for targeted *in situ* interfacial chemistries, as well as further highlighting additional design elements that must be considered to ensure molecular junction components do not decompose through carbocation elimination pathways.<sup>65</sup> Reassuringly, our observation that the S–C(*sp*<sup>3</sup>) bond in **Bn** does not readily cleave *in situ* during STM-BJ measurements further supports the conclusions of previous studies in molecular electronics which have utilized similar motifs without knowledge of their reactive potential (Figure S11).

## ■ ASSOCIATED CONTENT

### SI Supporting Information

The Supporting Information is available free of charge at <https://pubs.acs.org/doi/10.1021/acs.nanolett.5c01893>.

Additional experimental details; synthetic, conductance, and computational data; and <sup>1</sup>H and <sup>13</sup>C{<sup>1</sup>H} NMR spectra for all new compounds (PDF)

## ■ AUTHOR INFORMATION

### Corresponding Authors

Daniel Hernangómez-Pérez – CIC nanoGUNE BRTA, 20018 Donostia-San Sebastián, Spain; [orcid.org/0000-0002-4277-0236](https://orcid.org/0000-0002-4277-0236); Email: [d.hernangomez@nanogune.eu](mailto:d.hernangomez@nanogune.eu)

María Camarasa-Gómez – Centro de Física de Materiales (CFM-MPC) CSIC-UPV/EHU, 20018 Donostia-San Sebastián, Spain; Email: [maria.camarasa@ehu.eus](mailto:maria.camarasa@ehu.eus)

Michael S. Inkpen – Department of Chemistry, University of Southern California, Los Angeles, California 90089, United States; [orcid.org/0000-0001-7339-8812](https://orcid.org/0000-0001-7339-8812); Email: [inkpen@usc.edu](mailto:inkpen@usc.edu)

### Authors

Jazmine Prana – Department of Chemistry, University of Southern California, Los Angeles, California 90089, United States

Luana Zagami – Department of Chemistry, University of Southern California, Los Angeles, California 90089, United States

Kelly Yan – Department of Chemistry, University of Southern California, Los Angeles, California 90089, United States

Complete contact information is available at:

<https://pubs.acs.org/doi/10.1021/acs.nanolett.5c01893>

### Notes

The authors declare no competing financial interest.

## ■ ACKNOWLEDGMENTS

This work was primarily supported by funding from the University of Southern California (USC). D.H.-P. is grateful for funding from the Diputación Foral de Gipuzkoa through Grants 2023-FELL-000002-01 and 2024-FELL-000009-01. M.C.-G. acknowledges support from the Diputación Foral de Gipuzkoa through Grant 2024-FELL-000007-01 and from the Gobierno Vasco-UPV/EHU Project No. IT1569-22. M.C.-G. and D.H.-P. acknowledge the technical and human support provided by the DIPC Supercomputing Center. Instrumentation in the USC Chemistry Instrument Facility was acquired with support from the USC Research and Innovation Instrumentation Award Program. Additionally, funds provided by the National Science Foundation (DBI-0821671, CHE-0840366) and National Institutes of Health (S10 RR25432)

supported the acquisition of the NMR spectrometers used in our work.

## ■ REFERENCES

- (1) Vogt, C.; Weckhuysen, B. M. The Concept of Active Site in Heterogeneous Catalysis. *Nature Rev. Chem.* **2022**, *6* (2), 89–111.
- (2) Friend, C. M.; Xu, B. Heterogeneous Catalysis: A Central Science for a Sustainable Future. *Acc. Chem. Res.* **2017**, *50* (3), 517–521.
- (3) Chidsey, C. E. D. Free Energy and Temperature Dependence of Electron Transfer at the Metal-Electrolyte Interface. *Science* **1991**, *251* (4996), 919–922.
- (4) Bain, C. D.; Whitesides, G. M. Molecular-Level Control over Surface Order in Self-Assembled Monolayer Films of Thiols on Gold. *Science* **1988**, *240* (4848), 62–63.
- (5) Sullivan, T. P.; Huck, W. T. S. Reactions on Monolayers: Organic Synthesis in Two Dimensions. *Eur. J. Org. Chem.* **2003**, *2003* (1), 17–29.
- (6) Wink, T.; Van Zuilen, S. J.; Bult, A.; Van Bennekom, W. P. Self-Assembled Monolayers for Biosensors. *Analyst* **1997**, *122* (4), 43R–50R.
- (7) Bullock, R. M.; Das, A. K.; Appel, A. M. Surface Immobilization of Molecular Electrocatalysts for Energy Conversion. *Chem.—Eur. J.* **2017**, *23* (32), 7626–7641.
- (8) Love, J. C.; Estroff, L. A.; Kriebel, J. K.; Nuzzo, R. G.; Whitesides, G. M. Self-Assembled Monolayers of Thiolates on Metals as a Form of Nanotechnology. *Chem. Rev.* **2005**, *105* (4), 1103–1170.
- (9) Xu, B.; Tao, N. J. Measurement of Single-Molecule Resistance by Repeated Formation of Molecular Junctions. *Science* **2003**, *301* (5637), 1221–1223.
- (10) Inkpen, M. S.; Liu, Z.; Li, H.; Campos, L. M.; Neaton, J. B.; Venkataraman, L. Non-Chemisorbed Gold–Sulfur Binding Prevails in Self-Assembled Monolayers. *Nat. Chem.* **2019**, *11*, 351–358.
- (11) Cheng, Z. L.; Skouta, R.; Vazquez, H.; Widawsky, J. R.; Schneebeli, S.; Chen, W.; Hybertsen, M. S.; Breslow, R.; Venkataraman, L. In Situ Formation of Highly Conducting Covalent Au–C Contacts for Single-Molecule Junctions. *Nat. Nanotechnol.* **2011**, *6* (6), 353–357.
- (12) Millar, D.; Venkataraman, L.; Doerrer, L. H. Efficacy of Au–Au Contacts for Scanning Tunneling Microscopy Molecular Conductance Measurements. *J. Phys. Chem. C* **2007**, *111* (47), 17635–17639.
- (13) Li, S.; Yu, H.; Chen, X.; Gewirth, A. A.; Moore, J. S.; Schroeder, C. M. Covalent Ag–C Bonding Contacts from Unprotected Terminal Acetylenes for Molecular Junctions. *Nano Lett.* **2020**, *20* (7), 5490–5495.
- (14) Zang, Y.; Pinkard, A.; Liu, Z.-F.; Neaton, J. B.; Steigerwald, M. L.; Roy, X.; Venkataraman, L. Electronically Transparent Au–N Bonds for Molecular Junctions. *J. Am. Chem. Soc.* **2017**, *139* (42), 14845–14848.
- (15) Ahn, S.; Aradhya, S. V.; Klausen, R. S.; Capozzi, B.; Roy, X.; Steigerwald, M. L.; Nuckolls, C.; Venkataraman, L. Electronic Transport and Mechanical Stability of Carboxyl Linked Single-Molecule Junctions. *Phys. Chem. Chem. Phys.* **2012**, *14* (40), No. 13841.
- (16) Starr, R. L.; Fu, T.; Doud, E. A.; Stone, I.; Roy, X.; Venkataraman, L. Gold–Carbon Contacts from Oxidative Addition of Aryl Iodides. *J. Am. Chem. Soc.* **2020**, *142* (15), 7128–7133.
- (17) Czyszczon-Burton, T. M.; Montes, E.; Prana, J.; Lazar, S.; Rothowe, N.; Chen, S. F.; Vázquez, H.; Inkpen, M. S.  $\alpha,\omega$ -Alkanedibromides Form Low Conductance Chemisorbed Junctions with Silver Electrodes. *J. Am. Chem. Soc.* **2024**, *146* (41), 28516–28526.
- (18) Stone, I. B.; Starr, R. L.; Hoffmann, N.; Wang, X.; Evans, A. M.; Nuckolls, C.; Lambert, T. H.; Steigerwald, M. L.; Berkelbach, T. C.; Roy, X.; Venkataraman, L. Interfacial Electric Fields Catalyze Ullmann Coupling Reactions on Gold Surfaces. *Chem. Sci.* **2022**, *13*, 10798–10805.
- (19) Kim, L.; Czyszczon-Burton, T. M.; Nguyen, K. M.; Stuke, S.; Lazar, S.; Prana, J.; Miao, Z.; Park, S.; Chen, S. F.; Inkpen, M. S. Low

Vapor Pressure Solvents for Single-Molecule Junction Measurements. *Nano Lett.* **2024**, *24* (32), 9998–10005.

(20) Prana, J.; Kim, L.; Czyszczon-Burton, T.; Homann, G.; Chen, S.; Miao, Z.; Camarasa-Gomez, M.; Inkpen, M. Lewis-Acid Mediated Reactivity in Single-Molecule Junctions. *J. Am. Chem. Soc.* **2024**, *146* (48), 33265–33275.

(21) Ghasemi, S.; Ornago, L.; Liasi, Z.; Johansen, M. B.; Von Buchwald, T. J.; Hillers-Bendtsen, A. E.; Van Der Poel, S.; Hölzel, H.; Wang, Z.; Amombo Noa, F. M.; Öhrström, L.; Mikkelsen, K. V.; Van Der Zant, H. S. J.; Lara-Avila, S.; Moth-Poulsen, K. Exploring the Impact of Select Anchor Groups for Norbornadiene/Quadricyclane Single-Molecule Switches. *J. Mater. Chem. C* **2023**, *11* (44), 15412–15418.

(22) Rashid, U.; Bro-Jørgensen, W.; Harilal, K.; Sreelakshmi, P.; Mondal, R. R.; Chittari Pisharam, V.; Parida, K. N.; Geetharani, K.; Hamill, J. M.; Kaliginedi, V. Chemistry of the Au–Thiol Interface through the Lens of Single-Molecule Flicker Noise Measurements. *J. Am. Chem. Soc.* **2024**, *146* (13), 9063–9073.

(23) Hendrich, C. M.; Sekine, K.; Koshikawa, T.; Tanaka, K.; Hashmi, A. S. K. Homogeneous and Heterogeneous Gold Catalysis for Materials Science. *Chem. Rev.* **2021**, *121* (14), 9113–9163.

(24) Abboud, J.-L. M.; Alkorta, I.; Dávalos, J. Z.; Müller, P.; Quintanilla, E. Thermodynamic Stabilities of Carbocations. *Advances in Physical Organic Chemistry* **2002**, *37*, 57–135.

(25) Stühr-Hansen, N. The Tert -Butyl Moiety—A Base Resistant Thiol Protecting Group Smoothly Replaced by the Labile Acetyl Moiety. *Synth. Commun.* **2003**, *33* (4), 641–646.

(26) Pijper, T. C.; Robertus, J.; Browne, W. R.; Feringa, B. L. Mild Ti-Mediated Transformation of t-Butyl Thio-Ethers into Thio-Acetates. *Org. Biomol. Chem.* **2015**, *13* (1), 265–268.

(27) Deng, J.-R.; González, M. T.; Zhu, H.; Anderson, H. L.; Leary, E. Ballistic Conductance through Porphyrin Nanoribbons. *J. Am. Chem. Soc.* **2024**, *146* (6), 3651–3659.

(28) Venkataraman, L.; Klare, J. E.; Nuckolls, C.; Hybertsen, M. S.; Steigerwald, M. L. Dependence of Single-Molecule Junction Conductance on Molecular Conformation. *Nature* **2006**, *442* (7105), 904–907.

(29) Miao, Z.; Quainoo, T.; Czyszczon-Burton, T. M.; Rothowe, N.; Parr, J. M.; Liu, Z.; Inkpen, M. S. Charge Transport across Dynamic Covalent Chemical Bridges. *Nano Lett.* **2022**, *22* (20), 8331–8338.

(30) Venkataraman, L.; Klare, J. E.; Tam, I. W.; Nuckolls, C.; Hybertsen, M. S.; Steigerwald, M. L. Single-Molecule Circuits with Well-Defined Molecular Conductance. *Nano Lett.* **2006**, *6* (3), 458–462.

(31) Fatemi, V.; Kamenetska, M.; Neaton, J. B.; Venkataraman, L. Environmental Control of Single-Molecule Junction Transport. *Nano Lett.* **2011**, *11* (5), 1988–1992.

(32) He, J.; Sankey, O.; Lee, M.; Tao, N.; Li, X.; Lindsay, S. Measuring Single Molecule Conductance with Break Junctions. *Faraday Discuss.* **2006**, *131* (0), 145–154.

(33) Sedrez, P. C.; Noriega Sanchez, C. J.; Da Silva, M. J.; Barbosa, J. R. Addendum to “Dielectric Constant of Mixtures of Carbon Dioxide and n-Dodecane Between 283 K and 343 K, *Int. J. Thermophys.* **41**, 26, 2020”: Complementary Results for Mixtures of Carbon Dioxide and Squalane Between 283 and 343 K. *Int. J. Thermophys.* **2020**, *41* (6), 69.

(34) Haynes, W. M. *CRC Handbook of Chemistry and Physics*; CRC Press, 2014.

(35) Clayden, J.; Greeves, N.; Warren, S. *Organic Chemistry*; Oxford University Press, 2012.

(36) Smoluchowski, R. Anisotropy of the Electronic Work Function of Metals. *Phys. Rev.* **1941**, *60* (9), 661–674.

(37) Sykes, E. C. H.; Mantoath, B. A.; Han, P.; Donhauser, Z. J.; Weiss, P. S. Substrate-Mediated Intermolecular Interactions: A Quantitative Single Molecule Analysis. *J. Am. Chem. Soc.* **2005**, *127* (19), 7255–7260.

(38) Costello, C. K.; Kung, M. C.; Oh, H.-S.; Wang, Y.; Kung, H. H. Nature of the Active Site for CO Oxidation on Highly Active Au/ $\gamma$ -Al<sub>2</sub>O<sub>3</sub>. *Appl. Catal. A: Gen.* **2002**, *232*, 159–168.

(39) Schoenbaum, C. A.; Schwartz, D. K.; Medlin, J. W. Controlling the Surface Environment of Heterogeneous Catalysts Using Self-Assembled Monolayers. *Acc. Chem. Res.* **2014**, *47* (4), 1438–1445.

(40) Li, G.; Wang, B.; Resasco, D. E. Solvent Effects on Catalytic Reactions and Related Phenomena at Liquid-Solid Interfaces. *Surf. Sci. Rep.* **2021**, *76* (4), No. 100541.

(41) Tsiper, E. V.; Soos, Z. G.; Gao, W.; Kahn, A. Electronic Polarization at Surfaces and Thin Films of Organic Molecular Crystals: PTCDA. *Chem. Phys. Lett.* **2002**, *360* (2), 47–52. 1

(42) Sorenson, S. A.; Patrow, J. G.; Dawlaty, J. M. Solvation Reaction Field at the Interface Measured by Vibrational Sum Frequency Generation Spectroscopy. *J. Am. Chem. Soc.* **2017**, *139* (6), 2369–2378.

(43) Orchanian, N. M.; Guizzo, S.; Steigerwald, M. L.; Nuckolls, C.; Venkataraman, L. Electric-Field-Induced Coupling of Aryl Iodides with a Nickel(0) Complex. *Chem. Commun.* **2022**, *58*, 12556–12559.

(44) Dutta Dubey, K.; Stuyver, T.; Kalita, S.; Shaik, S. Solvent Organization and Rate Regulation of a Menshutkin Reaction by Oriented External Electric Fields Are Revealed by Combined MD and QM/MM Calculations. *J. Am. Chem. Soc.* **2020**, *142* (22), 9955–9965.

(45) Hollenstein, S.; Laube, T. Crystal Structure of the Tert-Butyl Cation. *J. Am. Chem. Soc.* **1993**, *115* (16), 7240–7245.

(46) Aziz, M.; Prindle, C. R.; Lee, W.; Zhang, B.; Schaack, C.; Steigerwald, M. L.; Zandkarimi, F.; Nuckolls, C.; Venkataraman, L. Evaluating the Ability of External Electric Fields to Accelerate Reactions in Solution. *J. Phys. Chem. B* **2024**, *128* (39), 9553–9560.

(47) Otomo, T.; Suzuki, H.; Iida, R.; Takayanagi, T. SN1 Reaction Mechanisms of Tert-Butyl Chloride in Aqueous Solution: What Can Be Learned from Reaction Path Search Calculations and Trajectory Calculations for Small Hydrated Clusters? *Comp. Theor. Chem.* **2021**, *1201*, No. 113278.

(48) Olah, G. A. Carbocations and Electrophilic Reactions. *Angew. Chem., Int. Ed. Engl.* **1973**, *12* (3), 173–212.

(49) Lifshitz, C. Tropylium Ion Formation from Toluene: Solution of an Old Problem in Organic Mass Spectrometry. *Acc. Chem. Res.* **1994**, *27* (5), 138–144.

(50) Sharma, D. K. S.; Kebarle, P. Stability and Reactivity of the Benzyl and Tropylium Cations in the Gas Phase. *Can. J. Chem.* **1981**, *59* (11), 1592–1601.

(51) Leary, E.; Zotti, L. A.; Miguel, D.; Márquez, I. R.; Palomino-Ruiz, L.; Cuerva, J. M.; Rubio-Bollinger, G.; González, M. T.; Agrait, N. The Role of Oligomeric Gold–Thiolate Units in Single-Molecule Junctions of Thiol-Anchored Molecules. *J. Phys. Chem. C* **2018**, *122* (6), 3211–3218.

(52) He, J.; Chen, F.; Liddell, P. A.; Andréasson, J.; Straight, S. D.; Gust, D.; Moore, T. A.; Moore, A. L.; Li, J.; Sankey, O. F.; Lindsay, S. M. Switching of a Photochromic Molecule on Gold Electrodes: Single-Molecule Measurements. *Nanotechnology* **2005**, *16* (6), 695–702.

(53) Bowers, C. M.; Rappoport, D.; Baghbanzadeh, M.; Simeone, F. C.; Liao, K.-C.; Semenov, S. N.; Žaba, T.; Cyganik, P.; Aspuru-Guzik, A.; Whitesides, G. M. Tunneling across SAMs Containing Oligophenyl Groups. *J. Phys. Chem. C* **2016**, *120* (21), 11331–11337.

(54) Sangtarash, S.; Vezzoli, A.; Sadeghi, H.; Ferri, N.; O’Brien, H. M.; Grace, I.; Bouffier, L.; Higgins, S. J.; Nichols, R. J.; Lambert, C. J. Gateway State-Mediated, Long-Range Tunneling in Molecular Wires. *Nanoscale* **2018**, *10* (6), 3060–3067.

(55) Vazquez, H.; Skouta, R.; Schneebeli, S.; Kamenetska, M.; Breslow, R.; Venkataraman, L.; Hybertsen, M. S. Probing the Conductance Superposition Law in Single-Molecule Circuits with Parallel Paths. *Nat. Nanotechnol.* **2012**, *7* (10), 663–667.

(56) Park, Y. S.; Widawsky, J. R.; Kamenetska, M.; Steigerwald, M. L.; Hybertsen, M. S.; Nuckolls, C.; Venkataraman, L. Frustrated Rotations in Single-Molecule Junctions. *J. Am. Chem. Soc.* **2009**, *131* (31), 10820–10821.

- (57) Batra, A.; Darancet, P.; Chen, Q.; Meisner, J. S.; Widawsky, J. R.; Neaton, J. B.; Nuckolls, C.; Venkataraman, L. Tuning Rectification in Single-Molecular Diodes. *Nano Lett.* **2013**, *13* (12), 6233–6237.
- (58) Blum, V.; Gehrke, R.; Hanke, F.; Havu, P.; Havu, V.; Ren, X.; Reuter, K.; Scheffler, M. Ab Initio Molecular Simulations with Numeric Atom-Centered Orbitals. *Comput. Phys. Commun.* **2009**, *180* (11), 2175–2196.
- (59) Camarasa-Gómez, M.; Hernangómez-Pérez, D.; Evers, F. Spin–Orbit Torque in Single-Molecule Junctions from Ab Initio. *J. Phys. Chem. Lett.* **2024**, *15* (21), 5747–5753.
- (60) Arnold, A.; Weigend, F.; Evers, F. Quantum Chemistry Calculations for Molecules Coupled to Reservoirs: Formalism, Implementation, and Application to Benzenedithiol. *J. Chem. Phys.* **2007**, *126* (17), No. 174101.
- (61) Bagrets, A. Spin-Polarized Electron Transport Across Metal–Organic Molecules: A Density Functional Theory Approach. *J. Chem. Theor. Comp.* **2013**, *9* (6), 2801–2815.
- (62) Thoss, M.; Evers, F. Perspective: Theory of Quantum Transport in Molecular Junctions. *J. Chem. Phys.* **2018**, *148* (3), No. 30901.
- (63) Evers, F.; Korytár, R.; Tewari, S.; Van Ruitenbeek, J. M. Advances and Challenges in Single-Molecule Electron Transport. *Rev. Mod. Phys.* **2020**, *92* (3), No. 35001.
- (64) Inman, C. E.; Reed, S. M.; Hutchison, J. E. In Situ Deprotection and Assembly of S-Tritylalkanethiols on Gold Yields Monolayers Comparable to Those Prepared Directly from Alkanethiols. *Langmuir* **2004**, *20* (21), 9144–9150.
- (65) Zagami, L.; Avedian, C.; Sharma, M.; Fraire, A.; Olivar, C.; Hernangómez-Pérez, D.; Inkpen, M. Isotropically Conducting Tetraaryl Osmium(IV), Silane, and Methane Molecular Wire Junctions. *ChemRxiv Preprint*, DOI: 10.26434/chemrxiv-2025-cjj3v (accessed 2025–03–26).